Published in final edited form as:
J Biol Chem. 2006 November 17; 281(46): 35156–35166. doi:10.1074/jbc.M606409200.

Loss of CNGB1 Protein Leads to Olfactory Dysfunction and Subciliary Cyclic Nucleotide-gated Channel Trapping[*,s]

Stylianos Michalakis[‡,1], **Johannes Reisert**[§,1], **Heidi Geiger**[‡], **Christian Wetzel**[¶], **Xiangang Zong**[‡], **Jonathan Bradley**[§], **Marc Spehr**[¶], **Sabine Hüttl**[‡], **Andrea Gerstner**[‡], **Alexander Pfeifer**[‡], **Hanns Hatt**[¶], **King-Wai Yau**[§], and **Martin Biel**[‡,2]

[‡] Department Pharmazie, Zentrum für Pharmaforschung, Ludwig-Maximilians Universität München, D-81377 München, Germany

[§] Department of Neuroscience, Johns Hopkins University School of Medicine, Baltimore, Maryland 21205

[¶] Lehrstuhl für Zellphysiologie, Ruhr-Universität Bochum, D-44780 Bochum, Germany

Abstract

Olfactory receptor neurons (ORNs) employ a cyclic nucleotide-gated (CNG) channel to generate a receptor current in response to an odorant-induced rise in cAMP. This channel contains three types of subunits, the principal CNGA2 subunit and two modulatory subunits (CNGA4 and CNGB1b). Here, we have analyzed the functional relevance of CNGB1 for olfaction by gene targeting in mice. Electro-olfactogram responses of CNGB1-deficient ($CNGB1^{-/-}$) mice displayed a reduced maximal amplitude and decelerated onset and recovery kinetics compared with wild-type mice. In a behavioral test, $CNGB1^{-/-}$ mice exhibited a profoundly decreased olfactory performance. Electrophysiological recordings revealed that ORNs of $CNGB1^{-/-}$ mice weakly expressed a CNG current with decreased cAMP sensitivity, very rapid flicker-gating behavior and no fast modulation by Ca^{2+}-calmodulin. Co-immunoprecipitation confirmed the presence of a CNGA2/CNGA4 channel in the olfactory epithelium of $CNGB1^{-/-}$ mice. This CNGA2/CNGA4 channel was targeted to the plasma membrane of olfactory knobs, but failed to be trafficked into olfactory cilia. Interestingly, we observed a similar trafficking defect in mice deficient for the CNGA4 subunit. In conclusion, these results demonstrate that CNGB1 has a dual function *in vivo*. First, it endows the olfactory CNG channel with a variety of biophysical properties tailored to the specific requirements of olfactory transduction. Second, together with the CNGA4 subunit, CNGB1 is needed for ciliary targeting of the olfactory CNG channel.

Cyclic nucleotide-gated (CNG)[3] channels are molecular switches converting receptor-mediated increases in cytosolic concentrations of cAMP or cGMP into an influx of cations. The channels play a key role in visual and olfactory transductions. The CNG channel involved in olfaction is expressed at high density in the sensory cilia of olfactory receptor neurons

[s]The on-line version of this article (available at http://www.jbc.org) contains supplemental Figs. S1 and S2.

[*]This work was supported in part by the Deutsche Forschungsgemeinschaft (to M. B. and A. G.) and Grant DC06904 from the National Institutes of Health (to K.-W. Y.).

[2]To whom correspondence should be addressed: Dept. Pharmazie, Pharmakologie für Naturwissenschaften, Ludwig-Maximilians-Universität München, Butenandtstr. 7, D-81377 München, Germany. Tel.: 49-89-2180-77327; Fax: 49-89-2180-77326; mbiel@cup.unimuenchen.de.

[1]Both authors contributed equally to this work.

Supplemental Material can be found at: http/www.jbc.org/content/suppl/2006/09/18/M606409200.DC1.html

[3]The abbreviations used are: CNG, cyclic nucleotide-gated; ORN, olfactory receptor neurons; PBS, phosphate-buffered saline; EOG, electro-olfactograms; CaM, calmodulin.

(ORNs) where it is activated by an odorant-induced rise of cAMP. When open, the channel conducts mainly Ca^{2+} and Na^{+} (1,2). The subsequent rise in internal Ca^{2+}, in turn, opens a Ca^{2+} -activated Cl^{-} channel, which confers an inward current and acts as an efficient amplifier of the primary CNG current (3–5). The combined CNG and Cl^{-} currents depolarize the ORN, initiating action potentials. Ca^{2+} entering the cell through CNG channels also serves as negative feedback modulator of signal transduction (6). Ca^{2+} reduces the cAMP sensitivity of the olfactory CNG channel through interaction with calmodulin (CaM) bound to the channel (7, 8). The olfactory CNG channel is a heterotetramer composed of three homologous subunits, CNGA2, CNGA4, and CNGB1b that are assembled in a 2:1:1 stoichiometry (9). Whereas the CNGA2 subunit can form functional homomeric channels when expressed heterologously, the CNGA4 and CNGB1b subunits only produce functional channels as heteromers with CNGA2. However, when expressed together with CNGA2, CNGA4 and CNGB1b confer a number of channel properties such as single channel flickering, increase in cAMP sensitivity and rapid Ca^{2+}-CaM modulation (10–14). The *CNGB1* gene is also transcribed in other tissues including brain, sperm and retina (15–18). CNGB1a, a splice variant expressed in the retina, assembles with CNGA1 to form the functional CNG channel of rod photoreceptors (19–21). Previously we have shown that mice deficient in the *CNGB1* gene ($CNGB1^{-/-}$) suffer from a primary loss of rod photoreceptor function and develop a progressive retinal degeneration resembling human retinitis pigmentosa. This severe phenotype results from the fact that rod photoreceptors fail to produce substantial levels of homomeric CNGA1 channels and/or are incapable of targeting such channels to the outer segment plasma membrane in the absence of CNGB1 (22).

Here, we sought to investigate the physiological role of CNGB1 in olfaction. We find that in the absence of CNGB1, ORNs express a heteromeric CNGA2/CNGA4 channel with biophysical properties that are significantly different from those of wild-type channels. Moreover, this channel is sensitive to proteasome-mediated degradation and is not substantially targeted to the cilia. As a consequence, CNGB1-deficient mice reveal a severely impaired olfactory performance. We also find that CNG channels deficient for the second “modulatory” subunit, CNGA4, fail to be targeted to the ciliary membrane. Thus, olfactory neurons possess a quality control system that ensures that only correctly assembled CNG channels are used for sensory transduction.

EXPERIMENTAL PROCEDURES

Animals

The generation of $CNGB1^{-/-}$ mice has been described (22). For all experiments, age-matched $CNGB1^{+/+}$, $CNGB1^{+/-}$, and $CNGB1^{-/-}$ mice on a hybrid 129Sv and C57BL/6N background were used. $CNGA3^{-/-}$/$CNGB1^{-/-}$ double knock-out mice were generated by cross-breeding of $CNGB1^{-/-}$ with $CNGA3^{-/-}$ mice (23). The animals were treated in accordance to both German legislation and the United States National Institutes of Health guidelines on the protection of animals.

Generation of Antibodies

Polyclonal antibodies directed against a sequence in the C terminus of the murine CNGA2 or the murine CNGA4 protein (C-AbmCNGA2: KQNHEDDY-LSDGINTPE; C-AbmCNGA4: REWPMPDDMGEADDEAE) were generated by standard techniques in rabbit and guinea pig, respectively (Gramsch Laboratories). C-AbmCNGA2 and C-AbmCNGA4 specifically detected the respective CNG channel subunit and showed no cross-reactivity to the other CNG channel subunits.

Histology

Adult mice were deeply anesthetized with ether and subsequently perfusion fixed (4% paraformaldehyde in 0.1 M phosphate buffered saline (PBS)). Olfactory turbinates were dissected, immersion-fixed for additional 2 h in 4% paraformaldehyde, cryoprotected in 30% sucrose, subsequently embedded in tissue-freezing medium (OCT, Sakura Finetek, Japan) and sectioned by cryostat. 12-μm thick coronal sections were thaw-mounted on glass slides (Superfrost Plus, Roth, Germany), air-dried and stored at −30 °C until used. Semithin sections of Epon-embedded olfactory turbinates (Epon 812, Fluka, Switzerland) were stained with toluidine blue (Fluka) and examined using light microscopy (Zeiss Axioskop 2 with HMRc-camera).

We quantified the epithelial thickness using digital images taken (at ×400 magnification) from coronal sections through the olfactory epithelia of litter-matched wild-type and knock-out mice (n = 3– 4 for each genotype). Measurements were performed on both sides of the nasal cavity at two positions (A left/A right and P left/P right). Position A was just adjacent to the posterior end of the vomeronasal organ, P was localized 400 μm posterior to A. The thickness of the epithelium was measured from the epithelial surface to the basal lamina using the Axiovision software measurement tool (Zeiss). For each position three consecutive slices were analyzed and averaged.

Immunohistochemistry

The sections were hydrated in PBS, post-fixed for 15 min (4% paraformaldehyde in PBS), and blocked for 3–4 h at room temperature (10% normal goat (NGS) or normal chicken serum (NCS), 0.5% Triton X-100 in PBS), followed by incubation overnight (16 h) at room temperature with primary antibodies in 5% NGS (or NCS), 0.25% Triton-X in PBS. After washing in 2% NGS (or NCS) in PBS sections were incubated for 1 h at room temperature with secondary antibodies in washing solution, then washed and mounted with aqueous mounting medium (Permaflour, Beckman-Coulter). Primary antibodies used were: rabbit anti-adenylyl cyclase III (sc-588, 1:400; Santa Cruz Biotechnologies), rabbit anti-CNGA3 (1:1000; (23)), C-AbmCNGA4 (1:250), rabbit C-AbmCNGB1 (1:400; (22)) rabbit anti-GC-D (1:500; gift from Dr. D. L. Garbers, University of Texas), goat anti-OMP (1:200; gift from Dr. F. Margolis, University of Maryland), and chicken anti-PDE2 (1:100; gift from Dr. J. Beavo, University of Washington). For detection of CNGA2 we used C-AbmCNGA2 (1:300). The same results were obtained with goat anti-CNGA2 (sc-13700, 1:250, Santa Cruz Biotechnologies) (not shown). Secondary detection: donkey FITC or Cy2 anti-rabbit IgG or anti-chicken, donkey TexasRed anti-guinea pig IgG and donkey biotin anti-goat IgG (all Jackson Immunoresearch Europe, UK), DY-547 streptavidin (Dyomics, Germany). Direct fluorescence microscopy was carried out using primary antibodies labeled with DY-547-NHS ester or DY-631-NHS ester (Dyomics). Sections were analyzed with a LSM 510 Meta confocal laser microscope (Zeiss, Germany).

Western Blot and Co-immunoprecipitation

HEK293 cells were transfected with CNG channel cDNAs (8,24) or a cDNA of rat CNGB1b that lacks all exons downstream of exon 25, and membrane proteins were isolated as previously described (25). Membranes from murine olfactory epithelia were prepared using the mechanical agitation method described by Washburn *et al.* (26). Equal amounts of proteins were separated using 7–10% SDS-PAGE followed by Western blot analysis according to standard procedures. The antibodies were used in the following dilutions: anti-adenylyl cylase III (sc-588, 1:400), C-AbmC-NGA2 (1:1000), C-AbmCNGA4 (1:500), FPc21K (1:2500; gift from Dr. U. B. Kaupp, FZJ-IBI-1 Jülich, Germany), anti-tubulin (1:400; Dianova, Germany). Co-immunoprecipitation was performed as described previously (27). For immunoprecipitation 210 μg of olfactory membranes were incubated with 10 μg of C-

AbmCNGA2 or 10 μg of anti-PAK (control antibody; sc-882, Santa Cruz Biotechnologies). The immunoblot was probed with C-AbmCNGA4 (1:500).

Electrophysiology

Tissue was dissociated as described in Reisert *et al.* (28). Briefly, following euthanasia of the animal by methods approved by Johns Hopkins University, olfactory turbinates were removed from the nasal cavity, transferred to extracellular solution and stored at 4 °C until use. To aid dissociation, the olfactory epithelium was peeled off its supporting cartilage, incubated in extracellular solution containing 0.2 mg/ml trypsin (Sigma) for 30 min at 37 °C and thereafter transferred to a solution containing 0.4 mg/ml DNase I (Roche Applied Science), 140 mM NaCl, 2 mM $MgCl_2$. After gentle trituration, 700 μl of cell suspension were transferred to a recording chamber mounted on an inverted microscope and allowed to settle for 30 min.

Inside-out patches were excised from the dendritic knobs of ORNs. Often cilia were visible and could be sucked into the recording pipette before sealing. Recordings were performed as described previously (29). Recording from heterologously expressed CNG channels was performed as described (8,24).

Pipettes were pulled from standard wall borosilicate glass (Warner Instrument Corp., Hamden, CT) and fire-polished to give an open-pipette resistance of 7 MΩ or 13–15 MΩ for single channel recordings. Currents were recorded using an Axo-patch-1D amplifier, a Digidata interface and pClamp software (Axon Instruments, Inc.). All data were sampled at 500 Hz and low-pass-filtered at 100 Hz (8-pole Bessel). Only for the single channel recordings was the sampling rate 5 kHz, and currents were filtered at 0–1 kHz. The holding potential was −40 mV, except for the single channel recordings where a holding potential of −60 mV was used.

All solutions contained 10 mM HEPES, the pH was adjusted to 7.2 with NMDG. Most experiments were performed in 140 mM symmetrical NaCl solution, with 10 mM HEPES and 10 mM HEDTA. Adding 9.98 mM $CaCl_2$ yielded a free Ca^{2+} concentration of 67 μM. The inhibition of the CNG channel by Ca-CaM was investigated in a solution where 130 mM NaCl were replaced equimolarly by sodium methane sulfonate to minimize the Ca^{2+}-activated Cl^- current. Extracellular solution contained (in mM): NaCl 125, KCl 5, EGTA 10. Solution exchanges were applied by transferring the tip of the patch pipette across the interface of neighboring streams of solution using the Perfusion Fast-Step SF-77B solution changer (Warner Instrument Corp.).

EOG Recordings

The recordings were performed as described (30). In brief, the septal bone and the associated epithelium were placed in a recording chamber. Unipolar recording was achieved by placing an active electrode consisting of a Ringer's/agarose-filled teflon tube on the epithelium and connecting it with a silver/silver chloride wire to a DC amplifier (P18C, Grass Instrument Co.) referenced to an identical electrode grounding the bath. Odorants were delivered in the vapor phase using a custom-made olfactometer. 100 μl of a complex 100-component odorant mixture (Henkel 100; gift from Dr. T. Gerke, Henkel KGaA, Germany) (30,31), were diluted in bidistilled water in a 50-ml syringe, continuously streamed with air. This odorant was injected into a constant stream of humidified air that continuously superfused the epithelium. Signals were recorded on a chart recorder. Strip chart recordings were scanned and digitized using the measurement tool of the Zeiss Axiovision software (Zeiss). Response kinetics were analyzed according to the time between the onset of a response and its peak amplitude (time to peak). Additionally, recovery kinetics was analyzed using a double exponential fit.

Calcium Imaging

Calcium imaging was performed as described (30). Briefly, intracellular Ca^{2+} was monitored using fura-2/AM (Molecular Probes) dissolved in a stock solution (1 mM) consisting of Me_2SO and 20% Pluronic F-127 (Molecular Probes). Freshly dissociated ORNs were dye-loaded for 45 min (room temperature), washed with extracellular solution, and monitored on a Zeiss inverted microscope (×40 objective) equipped for ratiometric imaging (TillPhotonics, Germany). Fluorescence intensities after sequential illumination (340 nm and 380 nm; 75-ms pulses; 2-Hz cycle time) were captured by a cooled CCD camera(TillPhotonics). Knobs of individual ORNs were marked as regions of interest (ROI; Tillvision software) and the average pixel intensity within each ROI was digitized and stored on a PC. Only cells morphologically identified as ORNs (dendrite with knob and cilia) were included into analysis. The Ca^{2+}-dependent fluorescence signal was expressed as the f_{340}/f_{380} ratio and viewed as a function of time.

ORNs were focally stimulated by forskolin/odorants (5-s pulses; interstimulus intervals of 80 –150 s) using a custom-build six capillary tube application system (integrated suction; switching time essentially instantaneous; flow rates of 5 μl/s). Stimulus concentration refers to the concentration in each tube. Control experiments showed minimized background accumulation of stimuli and no “on/off” artifacts. Response kinetics were analyzed according to the time between the onset ($f_{340}/f_{380} \geq 15\%$ of base level) of a response and its peak amplitude. Recovery kinetics were analyzed using a single exponential fit and calculating its time constant (τ). Statistical analysis used two sample equal variance *t* tests.

Olfactory Performance Test

Single housed mice were food-deprived for 18 h. After a food pellet (V1534, 25 × 10 mm, Ssniff, Germany) was buried in the home cage (3 cm under the bedding), the mouse was allowed to search for the pellet. The time needed to localize the food pellet was measured. The test was terminated after the successful localization of the pellet or after 10 min of unsuccessful searching.

Open Field Test

Locomotor activity was measured in an infrared beam operated open field (25 × 25 × 25 cm, ActiMot-System, TSE, Bad Homburg, Germany). Each mouse was placed in the middle of the open field and monitored for 10 min. Total distance traveled (m), number of rearings, and speed (cm/s) were determined.

Odor Exposure for Fos Experiments

Mice were placed in a sealed housing cage (IVC, Techniplast, Germany). The cage was ventilated with fresh air continuously flowing at 3 liters/min for 30 min. Thereafter, mice were exposed to Henkel 100 equilibrated air (delivered at 3 liters/min to the cage). Odorant exposure occurred intermittently to minimize adaptation effects. Odors were presented seven times for 2 min with 3 min intervening fresh air intervals. Control mice received the same treatment, but with fresh air only. Two hours after exposure mice were anesthetized and perfusion-fixed as described above. 12-μm olfactory bulb sections were processed for Fos immunohistochemistry using a rabbit anti-Fos antibody (1:10000; Calbiochem). Immunoreactivity was visualized using the Vectastain ABC kit (Vector) and Ni-DAB Substrate Kit (Vector).

Proteasome Inhibition

4-week-old $CNGB1^{-/-}$ mice were intraperitonealy injected (10 μg/g of body-weight) with the specific and cell permeable proteasome inhibitor carbobenzoxy-L-leucyl-L-leucyl-L-leucinal (MG-132; Calbiochem, Germany). After an incubation time of 20 h, the mice were

anesthetized, perfusion-fixed, and the olfactory turbinates were isolated as described above. Another group of mice received two consecutive doses of MG-132 (10 μg/g of body weight; 24 h between the two applications), and again, after 20 h of incubation time the olfactory turbinates were removed as described above.

Statistics

All data are presented as means ± S.E. If not specified otherwise, data were analyzed by unpaired Student's *t* test. Statistical significance was accepted if $p < 0.05$.

RESULTS

Reduced Olfactory Performance in CNGB1$^{-/-}$ Mice

CNGB1$^{-/-}$ mice of both genders showed a delayed postnatal body weight increase compared with their CNGB1$^{+/-}$ and CNGB1$^{+/+}$ littermates (Fig. 1*A*). Even in the fourth postnatal week, a time point at which mice can be considered adult, the body weight of CNGB1$^{-/-}$ mice was about 30% lower than that of littermate control mice ($p < 0.0001$; CNGB1$^{-/-}$: 11.3 ± 0.5 g, ($n = 34$); CNGB1$^{+/-}$: 15.3 ± 0.3 g, ($n = 68$); CNGB1$^{+/+}$: 16.4 ± 0.5 g, ($n = 21$)). To test whether CNGB1$^{-/-}$ mice are impaired in olfaction we conducted an olfactory performance test. We found that CNGB1$^{-/-}$ mice were able to locate a hidden food pellet but needed about three times as long for this task as wild-type littermates (CNGB1$^{-/-}$: 438.4 ± 36.3 s, ($n = 28$); CNGB1$^{+/+}$: 148.4 ± 23.4 s, ($n = 17$); $p < 0.0001$) (Fig. 1*B*). Double knock-out mice deficient in CNGB1 and also CNGA3, a subunit expressed in a small subset of ORNs that appear to employ a cGMP-based transduction cascade (32), showed the same performance as CNGB1$^{-/-}$ mice (n.s.; 423.9 ± 78.8 s, ($n = 9$)) (Fig. 1*B*). This finding suggests that the ability of CNGB1$^{-/-}$ mice to smell was not conferred by CNGA3-expressing ORNs. More probably, it reflected the reduced activity of the primary, cAMP-mediated olfactory system. To exclude that the knock-out mice had an impaired exploratory activity we performed an open field test. Overall, CNGB1$^{-/-}$ mice had normal activity as measured by the total distance traveled (CNGB1$^{-/-}$: 6.6 m ± 0.5 m ($n = 9$); CNGB1$^{+/+}$: 5.5 m ± 0.4 m ($n = 8$); $p = 0.09$), the speed (CNGB1$^{-/-}$: 11.0 cm/s ± 0.8 cm/s ($n = 9$); CNGB1$^{+/+}$: 9.1 cm/s ± 0.7 cm/s ($n = 8$); $p = 0.09$) and the number of rearings (CNGB1$^{-/-}$: 268.6 ± 40.8 ($n = 9$); CNGB1$^{+/+}$: 245.8 ± 33.1 ($n = 8$); $p = 0.68$).

We next asked whether the morphology of the olfactory system was altered in the knock-out mice. The principal structure of the olfactory epithelium was unaffected by the deletion of CNGB1 (Fig. 2*A*). Moreover, the expression pattern of OMP, a marker protein for mature ORNs (33), was comparable in the olfactory epithelium of CNGB1$^{-/-}$ and wild-type mice (Fig. 2*B*). However, the olfactory epithelium of knock-out mice was consistently thinner (15 to 20%) than that of wild-type mice (thickness in 4-week-old mice: anterior position: CNGB1$^{-/-}$: 70.7 ± 0.3 μm ($n = 3$); CNGB1$^{+/+}$: 83.7 ± 1.3 μm; ($n = 3$), $p < 0.0001$; posterior position: CNGB1$^{-/-}$: 72.1 ± 2.6 μm ($n = 3$); CNGB1$^{+/+}$: 89.9 ± 2.5 μm; ($n = 3$); $p < 0.001$).

Compared with litter-matched wild types there was also an obvious decrease in the size of the olfactory bulb in CNGB1$^{-/-}$ mice (Fig. 3*A*). In contrast, the gross morphology of the olfactory bulb was not compromised, since all CNGB1-deficient mice analyzed showed the six well-known olfactory bulb layers (not shown). Moreover, tyrosine hydroxylase expression in the periglomerular cells was comparable in knock-out and control mice, indicating that olfactory bulbs of CNGB1$^{-/-}$ mice received afferent inputs from ORNs (Fig. 3*B*). To investigate the functionality of the olfactory system, we determined odor-evoked Fos activity in periglomerular neurons of the olfactory bulb. Fos is an immediate early gene product that is up-regulated in odor-activated periglomerular neurons in response to odorants (34). As expected, Fos protein expression detected by an anti-Fos antibody was enhanced in a number

of olfactory glomeruli after exposure to a complex 100-component odorant mixture (Henkel 100, Ref. 31) (Fig. 3*C*). Up-regulation of Fos was also observed in CNGB1$^{-/-}$ mice, however the number of Fos-stained glomeruli per slice (Fos^{+}) was smaller than in control mice (CNGB1$^{-/-}$: 22.7 ± 2.7 (n = 3); CNGB1$^{+/+}$: 31.3 ± 1.3 (n = 3), $p < 0.05$; Fig. 3*D*). This difference was probably attributable to the fact that the total number of glomeruli was also significantly reduced in CNGB1-deficient mice (CNGB1$^{-/-}$: 89.7 ± 1.6 (n = 3); CNGB1$^{+/+}$: 104.0 ± 4.0 (n = 3) glomeruli per slice; $p < 0.05$). Thus, the relative fraction of Fos^{+} glomeruli (%Fos^{+}) was not statistically different between both genotypes (p = 0.25; CNGB1$^{-/-}$: 25.2% ± 2.9% (n = 3); CNGB1$^{+/+}$: 30.3% ± 2.4% (n = 3) (Fig. 3*D*).

Odor Responses of ORNs in CNGB1-deficient Mice

To directly assess ORN function, we recorded odorant-evoked electro-olfactograms (EOGs). Fig. 4*A* shows representative EOG responses evoked by a 1-s pulse of Henkel 100 (1:1000, see “Experimental Procedures”) in adult litter-matched CNGB1$^{-/-}$ and CNGB1$^{+/+}$ mice. Both genotypes responded to the odorant mixture; however, the amplitude of the response was significantly smaller in the knock-out than in the control mice (CNGB1$^{-/-}$: 1.99 ± 0.56 mV; (n = 15); CNGB1$^{+/+}$: 5.31 ± 0.76 mV; (n = 10); $p < 0.005$) (Fig. 4, *A* and *B*). Moreover, the onset and offset of the response was profoundly slower in CNGB1$^{-/-}$ than in wild-type mice (Fig. 4*A* and Table 1). Ca^{2+}-imaging experiments on isolated ORNs confirmed this finding. After stimulation with forskolin, an activator of the adenylyl cyclase (Fig. 4*C*), or with Henkel 100 (not shown), ORNs of CNGB1$^{-/-}$ and wild-type mice showed a transient increase of the Ca^{2+} concentration in their dendritic knobs. As observed with the EOG response, the on- and off-kinetics of the Ca^{2+} wave were profoundly slower in knock-out than in control mice (Fig. 4*C* and Table 1). Moreover, the threshold for the induction of a Ca^{2+} signal was somewhat higher in CNGB1$^{-/-}$ than in wild-type mice. While in both genotypes more than 90% of the ORNs responded to 3 μM forskolin (CNGB1$^{-/-}$: 32 out of 35 ORNs; CNGB1$^{+/+}$: 33 out of 35 ORNs) the number of responders at 1 μM forskolin was lower in the knockouts (17 out of 35 ORNs) compared with the wild-type mice (25 out of 35 ORNs).

The Olfactory CNG Current in CNGB1$^{-/-}$ Mice Has a Reduced Density, Lower cAMP Affinity, and Extremely Rapid Single Channel Flickering

The experiments described so far indicated that ORNs of CNGB1$^{-/-}$ mice principally respond to odorants, but display a reduced sensitivity and altered response kinetics. We tested whether these changes could be correlated with altered properties of the CNG current in CNGB1$^{-/-}$ mice. We first compared the magnitudes of the two components of the olfactory receptor current (CNG and Ca^{2+}-activated Cl^{-} current) in excised patches from dendritic knobs of ORNs. Saturating concentrations of cAMP (1 mM) and Ca^{2+} (67 μM) induced robust currents in patches from both genotypes (Fig. 5, A and B). However, the mean CNG current was about 10 times smaller in knock-out mice than in controls (CNGB1$^{-/-}$: 23 ± 3 pA; (n = 9); CNGB1$^{+/+}$: 273 ± 49 pA; (n = 9); p < 0.005). By contrast, the maximal Cl^{-} current was virtually identical in both genotypes (Fig. 5C). As a consequence, the average ratio I_{CNG}/I_{Cl}^{-} was 1.64 ± 0.35 for CNGB1$^{+/+}$ and 0.16 ± 0.06 for CNGB1$^{-/-}$ mice ($p < 0.005$, n = 9). Additionally, the CNG current of CNGB1$^{-/-}$ mice revealed a lower sensitivity to cyclic nucleotides. The apparent affinity for cAMP was shifted by about 5-fold to a higher cAMP concentration (Fig. 5, *D–F* and Table 2). The cGMP sensitivity was decreased by a factor of three in CNG channels from CNGB1$^{-/-}$ cells compared with the control (Table 2). Overall, the cAMP and cGMP affinities of CNGB1$^{+/-}$ and CNGB1$^{-/-}$ channels were broadly consistent with those for heterologously expressed CNGA2 + A4 + B1b and CNGA2 + A4 channels (Table 2). Interestingly, at saturating cAMP concentration, current traces of knock-out mice frequently revealed an initial decay that was never observed in control currents (compare Fig. 5, *D* and *E*). A similar initial decay of the current was described for the heterologously expressed rat CNGA2/CNGA4 channels (35). The CNG channel in ORNs of wild-type mice showed rapid

opening and closing kinetics at the single-channel level (Fig. 5*G*). The single channel conductance determined from an all-point histogram was 23 ± 1 pS at −60 mV (n = 8). CNG channels of knock-out mice revealed an extremely pronounced flicker-gating behavior that prevented the determination of a single channel conductance (Fig. 5, *H* and *I*). A similar rapid flicker was reported for the heterologously expressed rat CNGA2/CNGA4 channel (36).

Absence of Fast Ca^{2+}-CaM-dependent Inhibition of CNG Channels of CNGB1$^{-/-}$ Mice

Feedback modulation by Ca^{2+}-CaM is a key feature of olfactory CNG channels. Indeed, incubation of excised patches from wild-type ORNs with 100 nM calmodulin and 100 μM Ca^{2+} induced a rapid inhibition of the cAMP-mediated current (τ_{fast} = 1.1 ± 0.1 s, τ_{slow} = 60 ± 33 s, n = 9) (Fig. 6*A*). For CNGB1$^{-/-}$ channels; however, the kinetics of current inhibition by the same concentrations of Ca^{2+} and calmodulin was slowed by almost 100-fold (τ = 107 ± 29 s, n = 3) (Fig. 6*B*). Similarly slow kinetics of Ca^{2+}-CaM-dependent inhibition was determined for the heterologously expressed CNGA2/CNGA4 channel (τ = 63 ± 11 s, n = 11) (Fig. 6*C*).

In conclusion, the biophysical properties of the CNG current of CNGB1$^{-/-}$ ORNs were consistent with the presence of a heteromeric CNGA2/CNGA4 channel. Moreover, the reduced cyclic nucleotide sensitivity of this channel together with the strongly decelerated kinetics of Ca^{2+}-CaM-dependent inhibition could explain the delayed onset and recovery of EOG responses in CNGB1$^{-/-}$ mice. However, the altered biophysical properties could not explain why the mean amplitude of the CNG current as well as the peak EOG response was dramatically reduced in the knock-out mice. To explore this important issue we analyzed the expression of olfactory CNG channel subunits at the protein level.

Requirement of CNGB1 for the Presence of CNGA2 and CNGA4 Subunits in the Cilia of ORNs

Antibodies specific for the N terminus (Fig. 7*A*) or the C terminus (not shown) of CNGB1 detected the 120-kDa CNGB1b protein in membrane fractions from wild type but not from CNGB1$^{-/-}$ mice. Notably, a truncated CNGB1b protein that theoretically could be encoded by the mutant CNGB1-locus was not detected in knock-out mice (Fig. 7*A*), confirming that the knock-out was complete. We performed co-immunoprecipitation experiments with olfactory membrane fractions to determine whether CNGA2 and CNGA4 coassembled in CNGB1$^{-/-}$ mice (Fig. 7*B*). Indeed, in immunoprecipitates obtained with an anti-CNGA2 antibody, CNGA4 was detected. However, the CNGA4 signal was profoundly weaker in the knock-out compared with wild-type mice suggesting that the total expression level of one or both of the subunits was decreased in the knockouts.

To further address this issue, we examined the subcellular localization of CNG channel subunits in the ORNs. Fig. 8 shows confocal scans of coronal sections through the mouse olfactory epithelium stained with specific antibodies against the three olfactory CNG channel subunits. An antibody against ACIII was used as a marker for the ciliary layer. In wild-type mice, all three olfactory CNG channel subunits were highly enriched in the cilia (Fig. 8, *A–D*; see also supplementary Fig. S1 for overview images showing CNGA2 and ACIII expression in a whole olfactory turbinate of wild-type and CNGB1$^{-/-}$ mice). The CNG channel subunits were also very faintly expressed in the somata of ORNs. In CNGB1$^{-/-}$ mice, CNGA2 and CNGA4 were not detectable in the ciliary layer (Fig. 8, *E* and *F*). However, protein levels of both subunits were increased in somata, dendrites, and knobs. As expected, staining with the anti-CNGB1 antibody yielded no signal at all (Fig. 8*G*). Expression of ACIII was not different between wild-type and CNGB1$^{-/-}$ mice, indicating that the cilia of ORNs developed normally in the knockouts (Fig. 8*H*). Moreover, the subpopulation of ORNs expressing the CNGA3 subunit and other components of a putative cGMP-mediated signaling pathway were normally represented in the olfactory epithelium of CNGB1$^{-/-}$ mice (supplemental Fig. S2). Importantly, there was no compensatory up-regulation of the number of these CNGA3-positive ORNs in

CNGB1$^{-/-}$ mice. We performed another series of staining with sections from mice lacking the CNGA4 subunit (37) (Fig. 8, *I–L*). Like in CNGB1$^{-/-}$ mice, CNG channel subunits were absent from the cilia, whereas ACIII was normally expressed in this cell compartment. Moreover, levels of CNGA2 and CNGB1 were increased in the somata and dendrites of CNGA4$^{-/-}$ mice. Together, these results indicated that, in the absence of either CNGB1 or CNGA4, the olfactory CNG channel fails to be routed to the cilia and accumulates in subciliary regions of the ORNs.

Specific Defect in Ciliary Targeting of CNGA2/CNGA4 Channels

Although CNGA2 and CNGA4 mRNA levels in the olfactory epithelium of CNGB1$^{-/-}$ mice are comparable to the wild-type (not shown), there is an apparent decrease in expression levels of these two channel subunits on the protein level (Fig. 7*B* and Fig. 8, *E* and *F*). The low CNG channel levels could be caused by an impairment in translation or ER processing. Another possible explanation would be rapid degradation of incorrectly localized CNG channels by the proteasome. To test for the latter idea, we treated CNGB1$^{-/-}$ mice either with the proteasome inhibitor MG-132 (38) (10 μg per g of body weight) or with buffer and analyzed the expression of CNGA2 and ACIII by immunohistochemistry (Fig. 9). After drug treatment, an accumulation of CNGA2 protein was observed in dendrites and knobs of drug-treated mice. By contrast, expression levels in the cilia were only slightly enhanced (compare Fig. 9, *A–C* with Fig. 9, *D–F*). After an additional day of proteasome inhibition, more protein accumulated in dendrites and knobs, but the levels of CNGA2 protein in the cilia did not further increase with respect to treatment with a single dose of MG-132 (Fig. 9, *G–I*). The same result was obtained for the CNGA4 subunit (not shown). The failure of knock-out mice to transport substantial amounts of CNGA2 and CNGA4 to the cilia was not caused by a general functional deficit of the cilia, because ciliary ACIII levels were normal in untreated mice (Fig. 9*B*) and were even up-regulated in MG-132-treated mice (Fig. 9, *E* and *H*).

DISCUSSION

Several lines of evidence indicate that the CNGB1b subunit is crucially required for normal olfactory function. First, CNGB1$^{-/-}$ mice have a delayed body weight development, presumably because of an olfactory deficit interfering with nursing and food intake. Second, CNGB1$^{-/-}$ mice perform worse than wild-type mice in an odor-based test of olfactory function. Third, the olfactory system of CNGB1$^{-/-}$ mice revealed morphological and biochemical alterations (thinner olfactory epithelium, smaller olfactory bulb) that have been also observed in other mouse lines displaying impaired olfaction, including CNGA2$^{-/-}$ mice (39,40), ACIII$^{-/-}$ mice (41) and G_{olf} $^{-/-}$ mice (42). Fourth, the EOG of CNGB1$^{-/-}$ mice has a significantly reduced amplitude and slowed onset and recovery kinetics. Finally, stimulus-induced Ca^{2+} transients in isolated ORNs of CNGB1$^{-/-}$ mice also reveal decelerated on- and off-kinetics compared with transients from wild-type ORNs.

The altered kinetics of the odorant response can be well explained by the particular biophysical properties of the CNG channel expressed in the ORNs of CNGB1$^{-/-}$ mice. We found that the apparent cAMP affinity of the CNGB1$^{-/-}$ current is about five times lower than that of the wild-type current. Thus, more cAMP (and thus, a higher odorant concentration) is required to activate the channel. As a consequence, the onset of the EOG and the Ca^{2+} transient would be delayed. The slow recovery of the odorant response can be explained by the fact that the CNGB1$^{-/-}$ current completely lacks fast inhibition by Ca^{2+}-CaM. With respect to this feature the CNGB1$^{-/-}$ current is very similar to the CNG current of CNGA4$^{-/-}$ mice that also lacks fast Ca^{2+}-CaM-dependent inhibition (37). Together, these findings correspond very well to recent heterologous expression experiments demonstrating that CNGB1b and CNGA4 subunits cooperate in mediating feedback modulation by Ca^{2+}-CaM (8,43). Absence of either

CNGB1b or CNGA4 results in a complete loss of fast feedback modulation and, hence, a profound deficit in odor adaptation.

The biophysical properties determined for the CNG channel of CNGB1$^{-/-}$ ORNs were consistent with the properties of the heterologously expressed CNGA2/CNGA4 channel. Co-immunoprecipitation experiments confirmed that both subunits indeed coassemble in the knock-out mice. Thus, in the absence of CNGB1b, CNGA2, and CNGA4 principally do assemble and form functional heteromeric channels in ORNs. Unexpectedly, however, the maximal current response of the knock-out ORNs was more than 10 times lower than the current measured in wild-type ORNs. The very rapid flicker, and thus the lower open probability, typical of CNGA2/CNGA4 channels may somewhat contribute to lower apparent peak current; however, this effect would not explain the profound reduction in CNG current observed. Immunobiological experiments clarified this conundrum. First, we found that the total amount of CNG channel protein was reduced in the knockouts. Moreover, the cilia of CNGB1$^{-/-}$ ORNs were essentially devoid of CNG channel subunits. The CNGA2 and CNGA4 proteins were only found in the somata, dendrites, and knobs of ORNs. Finally, the CNG proteins detected in CNGB1$^{-/-}$ ORNs may be partly degraded or trapped in cell compartments other than the cell membrane (*e.g.* endoplasmic reticulum, endosomes) and are, thus, not functional.

How is the olfactory CNG channel activated in CNGB1$^{-/-}$ mice? Because the ACIII is almost exclusively expressed in the cilia, cAMP produced in this compartment must diffuse to the knobs to activate the CNG channel. Alternatively, the components of the olfactory transduction machinery may be expressed at low levels in the knob (44,45), leaving open the option that locally produced cAMP activates the mislocalized CNGB1$^{-/-}$ channel. Because the CNGB1$^{-/-}$ channel shows much slower Ca^{2+}-CaM-dependent inhibition, once activated, it would remain in the open state for a longer time period than the wild-type channel. Thus, more Ca^{2+} than expected can enter the cell to activate the Ca^{2+}-dependent Cl^{-} channel. Such an amplification mechanism would compensate for lower channel protein levels and lower cAMP sensitivity of the knockout channel. This may explain why, despite the severely lowered CNG current, the EOG response is only about 2–3 times smaller in knock-out than in wild-type mice. It might also explain why CNGB1$^{-/-}$ mice can principally smell, though with reduced acuity and sensitivity. We cannot rule out that CNG channel-independent pathways might contribute to some extent to olfaction in CNGB1$^{-/-}$ mice. However, the finding that ACIII$^{-/-}$ mice are anosmic (41) and CNGA2$^{-/-}$ mice lack any cAMP-mediated odor responses (39,40) strongly argues against the notion that these CNG channel-independent pathways rely on cAMP.

A key finding of this study is that CNG channels lacking either the CNGB1b or the CNGA4 subunit fail to be targeted to the cilia of ORNs. CNG channels containing only two types of subunits (CNGA2/CNGA4 or CNGA2/CNGB1b) are assembled and also inserted into the plasma membrane of the knobs but do not localize to the cilia. Experiments with MG-132, a specific proteasome inhibitor, suggest that these channels are degraded by the action of the proteasome.

A recent study analyzed the ciliary trafficking of CNG channels in Madin-Darby canine kidney (MDCK) epithelial cells (46). MDCK cells contain a nonmotile primary cilium and show no endogenous CNG channel expression. By overexpressing wild-type and mutated olfactory CNG channel subunits in these cells a RV*X*P-motif in the C terminus of CNGB1b was identified that is necessary but not sufficient for ciliary targeting of CNGA2 (46). Interestingly, the same report showed that CNGA4 was not needed for ciliary CNG channel targeting in MDCK cells.

In contrast, our results indicate that both modulatory olfactory CNG subunits (CNGA4 and CNGB1b) are required to promote ciliary localization and to prevent degradation of the channel

in ORNs. Thus, unlike in MDCK cells, the structural determinant that is recognized by the targeting machinery of ORNs is formed by both CNGA4 and CNGB1b or even by all three CNG channel subunits. If one of the subunits is missing this specific interaction is no longer possible. Recently, a checkpoint protein (UNC-101) was identified that controls trafficking of odorant receptors into the olfactory cilia of *Caenorhabditis elegans* (47,48). Similar proteins may have evolved to control ciliary CNG channel targeting. A good candidate might be the motor protein KIF17 that was shown to interact with CNGB1b and to control CNG channel targeting in MDCK cells (46).

Interestingly, CNGB1$^{-/-}$ mice are also impaired in trafficking the CNGA1 subunit to rod outer segments. As a consequence, rods of CNGB1-deficient mice start to degenerate and die by apoptosis (22). Our finding that olfactory epithelium and olfactory bulbs of CNGB1$^{-/-}$ mice are undersized suggests that neurons in these tissues may also be subject to enhanced degeneration. Unlike photoreceptors, however, olfactory neurons are constantly replaced by differentiation of olfactory stem cells (49), a mechanism that probably can compensate for most of cell loss in CNGB1$^{-/-}$ mice. In any case, ORNs and photo-receptors have evolved an effective screening system to ensure that only correctly assembled CNG channels reach the plasma membrane of the cell compartment where sensory transduction takes place (*e.g.* ciliary membrane and outer segments, respectively). The existence of such a system underscores the crucial importance of optimal visual and olfactory performance for the competitiveness and, hence, the long-term survival of species.

Acknowledgments

We thank W. Grabowski for excellent technical assistance, R. R. Reed for the gift of CNGA4 knockout mice, J. Beavo, D. L. Garbers, U. B. Kaupp, F. Margolis, and F. Müller for the gift of antibodies used in this study. Henkel 100 was generously provided by T. Gerke, Henkel KGaA, Düsseldorf, Germany.

References

1. Nakamura T, Tsuru K, Miyamoto S. Neurosci Lett 1994;171:197–200. [PubMed: 8084489]
2. Frings S, Seifert R, Godde M, Kaupp UB. Neuron 1995;15:169–179. [PubMed: 7542461]
3. Kurahashi T, Yau KW. Nature 1993;363:71–74. [PubMed: 7683113]
4. Kleene SJ, Gesteland RC. J Neurosci 1991;11:3624–3629. [PubMed: 1941099]
5. Lowe G, Gold GH. Nature 1993;366:283–286. [PubMed: 8232590]
6. Matthews HR, Reisert J. Curr Opin Neurobiol 2003;13:469–475. [PubMed: 12965295]
7. Kurahashi T, Menini A. Nature 1997;385:725–729. [PubMed: 9034189]
8. Bradley J, Bönigk W, Yau KW, Frings S. Nat Neurosci 2004;7:705–710. [PubMed: 15195096]
9. Zheng J, Zagotta WN. Neuron 2004;42:411–421. [PubMed: 15134638]
10. Finn JT, Grunwald ME, Yau KW. Annu Rev Physiol 1996;58:395–426. [PubMed: 8815801]
11. Biel M, Zong X, Ludwig A, Sautter A, Hofmann F. Rev Physiol Biochem Pharmacol 1999;135:151–171. [PubMed: 9932483]
12. Kaupp UB, Seifert R. Physiol Rev 2002;82:769–824. [PubMed: 12087135]
13. Matulef K, Zagotta WN. Annu Rev Cell Dev Biol 2003;19:23–44. [PubMed: 14570562]
14. Bradley J, Reisert J, Frings S. Curr Opin Neurobiol 2005;15:343–349. [PubMed: 15922582]
15. Chen TY, Peng YW, Dhallan RS, Ahamed B, Reed RR, Yau KW. Nature 1993;362:764–767. [PubMed: 7682292]
16. Körschen HG, Illing M, Seifert R, Sesti F, Williams A, Gotzes S, Colville C, Muller F, Dose A, Godde M, Molday LL, Kaupp UB, Molday RS. Neuron 1995;15:627–636. [PubMed: 7546742]
17. Biel M, Zong X, Ludwig A, Sautter A, Hofmann F. J Biol Chem 1996;271:6349–6355. [PubMed: 8626431]
18. Wiesner B, Weiner J, Middendorff R, Hagen V, Kaupp UB, Weyand I. J Cell Biol 1998;142:473–484. [PubMed: 9679145]

19. Weitz D, Ficek N, Kremmer E, Bauer PJ, Kaupp UB. Neuron 2002;36:881–889. [PubMed: 12467591]
20. Zheng J, Trudeau MC, Zagotta WN. Neuron 2002;36:891–896. [PubMed: 12467592]
21. Zhong H, Molday LL, Molday RS, Yau KW. Nature 2002;420:193–198. [PubMed: 12432397]
22. Hüttl S, Michalakis S, Seeliger M, Luo D-G, Acar N, Geiger H, Hudl K, Mader R, Haverkamp S, Moser M, Pfeifer A, Gerstner A, Yau K-W, Biel M. J Neurosci 2005;25:130–138. [PubMed: 15634774]
23. Biel M, Seeliger M, Pfeifer A, Kohler K, Gerstner A, Ludwig A, Jaissle G, Fauser S, Zrenner E, Hofmann F. Proc Natl Acad Sci U S A 1999;96:7553–7557. [PubMed: 10377453]
24. Sautter A, Zong X, Hofmann F, Biel M. Proc Natl Acad Sci U S A 1998;95:4696–4701. [PubMed: 9539801]
25. Much B, Wahl-Schott C, Zong X, Schneider A, Baumann L, Moosmang S, Ludwig A, Biel M. J Biol Chem 2003;278:43781–43786. [PubMed: 12928435]
26. Washburn KB, Turner TJ, Talamo BR. Chem Senses 2002;27:635–642. [PubMed: 12200344]
27. Zong X, Eckert C, Yuan H, Wahl-Schott C, Abicht H, Fang L, Li R, Mistrik P, Gerstner A, Much B, Baumann L, Michalakis S, Zeng R, Chen Z, Biel M. J Biol Chem 2005;280:34224–34232. [PubMed: 16079136]
28. Reisert J, Bauer PJ, Yau KW, Frings S. J Gen Physiol 2003;122:349–363. [PubMed: 12939394]
29. Reisert J, Lai J, Yau KW, Bradley J. Neuron 2005;45:553–561. [PubMed: 15721241]
30. Spehr M, Wetzel CH, Hatt H, Ache BW. Neuron 2002;33:731–739. [PubMed: 11879650]
31. Wetzel CH, Oles M, Wellerdieck C, Kuczkowiak M, Gisselmann G, Hatt H. J Neurosci 1999;19:7426–7433. [PubMed: 10460249]
32. Meyer MR, Angele A, Kremmer E, Kaupp UB, Muller F. Proc Natl Acad Sci U S A 2000;97:10595–10600. [PubMed: 10984544]
33. Keller A, Margolis FL. J Neurochem 1975;24:1101–1106. [PubMed: 805214]
34. Guthrie KM, Anderson AJ, Leon M, Gall C. Proc Natl Acad Sci U S A 1993;90:3329–3333. [PubMed: 8475076]
35. Liman ER, Buck LB. Neuron 1994;13:611–621. [PubMed: 7522482]
36. Bönigk W, Bradley J, Muller F, Sesti F, Boekhoff I, Ronnett GV, Kaupp UB, Frings S. J Neurosci 1999;19:5332–5347. [PubMed: 10377344]
37. Munger SD, Lane AP, Zhong H, Leinders-Zufall T, Yau KW, Zufall F, Reed RR. Science 2001;294:2172–2175. [PubMed: 11739959]
38. Lee DH, Goldberg AL. J Biol Chem 1996;271:27280–27284. [PubMed: 8910302]
39. Brunet LJ, Gold GH, Ngai J. Neuron 1996;17:681–693. [PubMed: 8893025]
40. Baker H, Cummings DM, Munger SD, Margolis JW, Franzen L, Reed RR, Margolis FL. J Neurosci 1999;19:9313–9321. [PubMed: 10531436]
41. Wong ST, Trinh K, Hacker B, Chan GC, Lowe G, Gaggar A, Xia Z, Gold GH, Storm DR. Neuron 2000;27:487–497. [PubMed: 11055432]
42. Belluscio L, Gold GH, Nemes A, Axel R. Neuron 1998;20:69–81. [PubMed: 9459443]
43. Bradley J, Reuter D, Frings S. Science 2001;294:2176–2178. [PubMed: 11739960]
44. Menco BP, Bruch RC, Dau B, Danho W. Neuron 1992;8:441–453. [PubMed: 1550671]
45. Menco BP. Chem Senses 1997;22:295–311. [PubMed: 9218142]
46. Jenkins PM, Hurd TW, Zhang L, McEwen DP, Brown RL, Margolis B, Verhey KJ, Martens JR. Curr Biol 2006;16:1211–1216. [PubMed: 16782012]
47. Dwyer ND, Adler CE, Crump JG, L'Etoile ND, Bargmann CI. Neuron 2001;31:277–287. [PubMed: 11502258]
48. McClintock TS, Sammeta N. Neuroreport 2003;14:1547–1552. [PubMed: 14502073]
49. Graziadei PP, Monti Graziadei GA. J Neurocytol 1979;8:1–18. [PubMed: 438867]

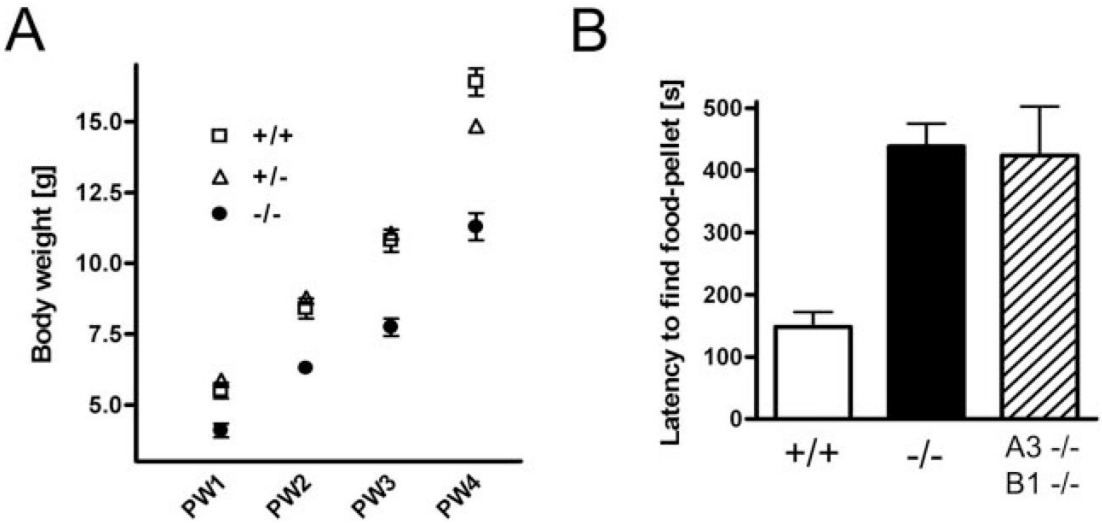

FIGURE 1. Delayed postnatal body weight increase and reduced olfactory performance in CNGB1$^{-/-}$ mice

A, body weight curves of littermate CNGB1$^{+/+}$ (*open squares; n* = 14 –28), CNGB1$^{+/-}$ (*open triangles; n* = 14 – 82), and CNGB1$^{-/-}$ (*filled circles; n* = 12–58) mice from the first postnatal week (*PW*) to PW4. The data for female and male mice were pooled. *B*, CNGB1$^{-/-}$ and CNGA3$^{-/-}$/CNGB1$^{-/-}$ double knock-out mice reveal a strongly increased mean latency to localize a hidden food pellet in an olfactory task.

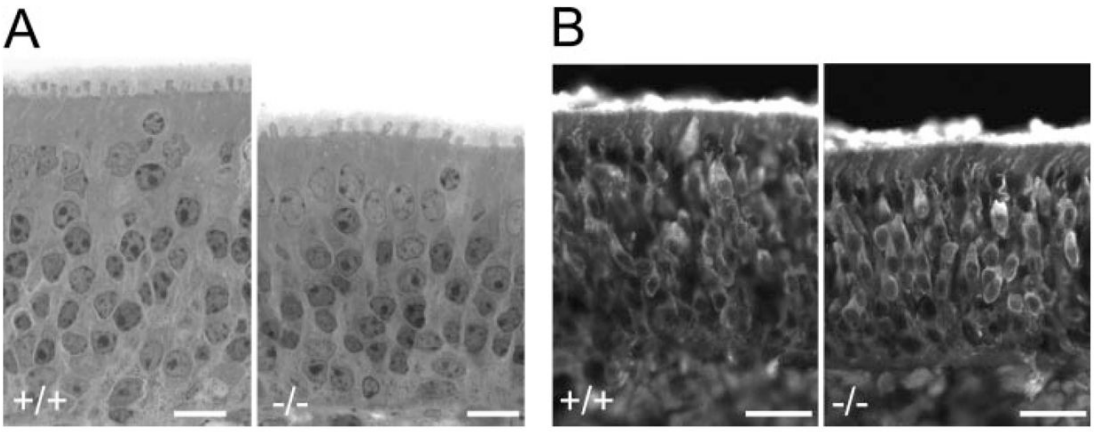

FIGURE 2. Morphology of the olfactory epithelium of wild-type and CNGB1$^{-/-}$ mice

A, toluidine blue-stained vertical semithin sections through the olfactory epithelium (turbinate IV) of CNGB1$^{+/+}$ and CNGB1$^{-/-}$ mice (litter-matched, 10-week-old). *B*, vertical sections through the olfactory epithelium of CNGB1$^{+/+}$ and CNGB1$^{-/-}$ mice immunostained with an antibody specific for the olfactory marker protein. *Scale bars* are 10 μm (*A*) and 20 μm (*B*).

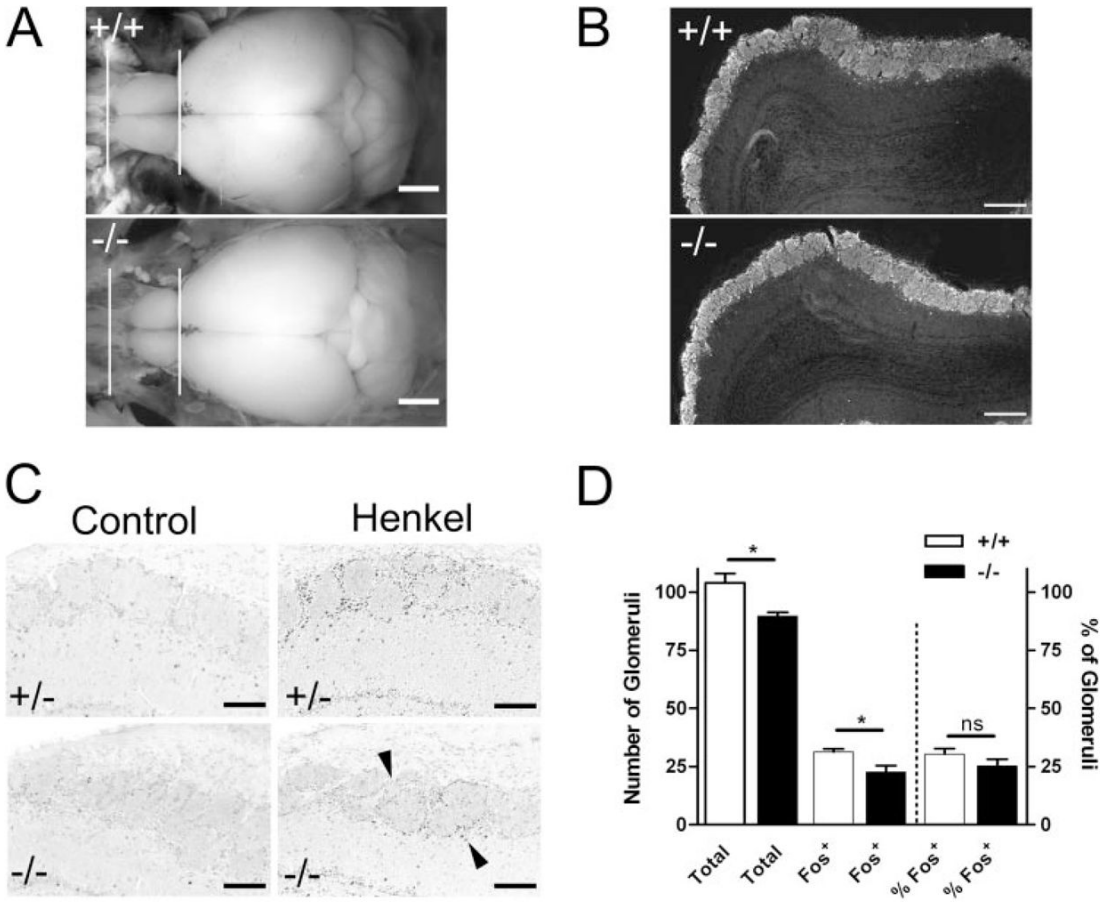

FIGURE 3. The olfactory bulb of CNGB1$^{-/-}$ mice is smaller than that of wild-type mice but reveals functional activity

A, gross brain morphology of litter-matched 4-week-old CNGB1$^{+/+}$ and CNGB1$^{-/-}$ mice. The *white lines* indicate the length of the wild-type olfactory bulb. *B*, coronal sections through the olfactory bulb of CNGB1$^{+/+}$and CNGB1$^{-/-}$ mice stained with anti-tyrosine hydroxylase antibody. *C*, odor-induced Fos expression in periglomerular neurons in CNGB1$^{+/-}$ and CNGB1$^{-/-}$ mice after incubation of the mice with fresh air (*left panel*) or air-saturated with a 100-compound odor mixture (Henkel 100) (*right panel*). The *arrowheads* point to knock-out glomeruli displaying Fos expression. *D*, quantification of total and Fos-positive (Fos^{+}) glomeruli in slices from identical regions of the olfactory bulb of CNGB1$^{+/+}$ (*white bars; n* = 3) and CNGB1$^{-/-}$ (*black bars; n* = 3) mice. Whereas the total number of glomeruli and the number of Fos^{+} glomeruli per slice is smaller in CNGB1$^{-/-}$ mice the fraction of Fos^{+} glomeruli (%Fos^{+}) is identical between both genotypes. *ns*, not significant. *, $p < 0.05$. *Scale bars* are 2 mm (*A*), 200 μm (*B*), and 50 μm (*C*).

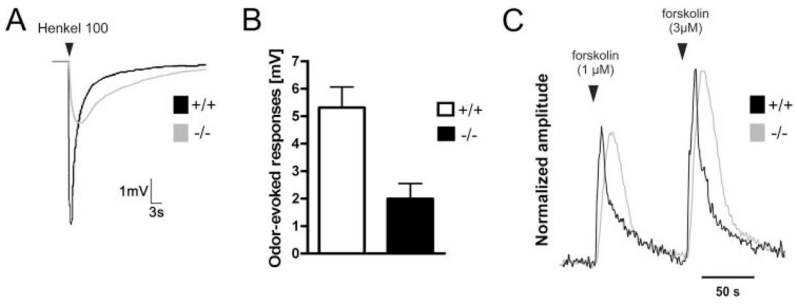

FIGURE 4. Significantly altered odor responses in CNGB1$^{-/-}$ mice

A, representative EOG traces of CNGB1$^{+/+}$ (*black*) and CNGB1$^{-/-}$ (*gray*) mice. Responses were obtained after a 1-s pulse of Henkel 100. *B*, mean peak amplitudes of Henkel 100-evoked responses were significantly smaller in CNGB1$^{-/-}$ (*black bar; n* = 15) than in CNGB1$^{+/+}$mice (*white bar; n* = 10) ($p < 0.005$). *C*, representative traces of ratiofluorometric recordings from CNGB1$^{+/+}$ (*black*) and CNGB1$^{-/-}$ (*gray*) ORN knobs revealed delayed Ca^{2+} -signals in knock-out mice. Traces were normalized to the maximum response allowing comparison of response kinetics.

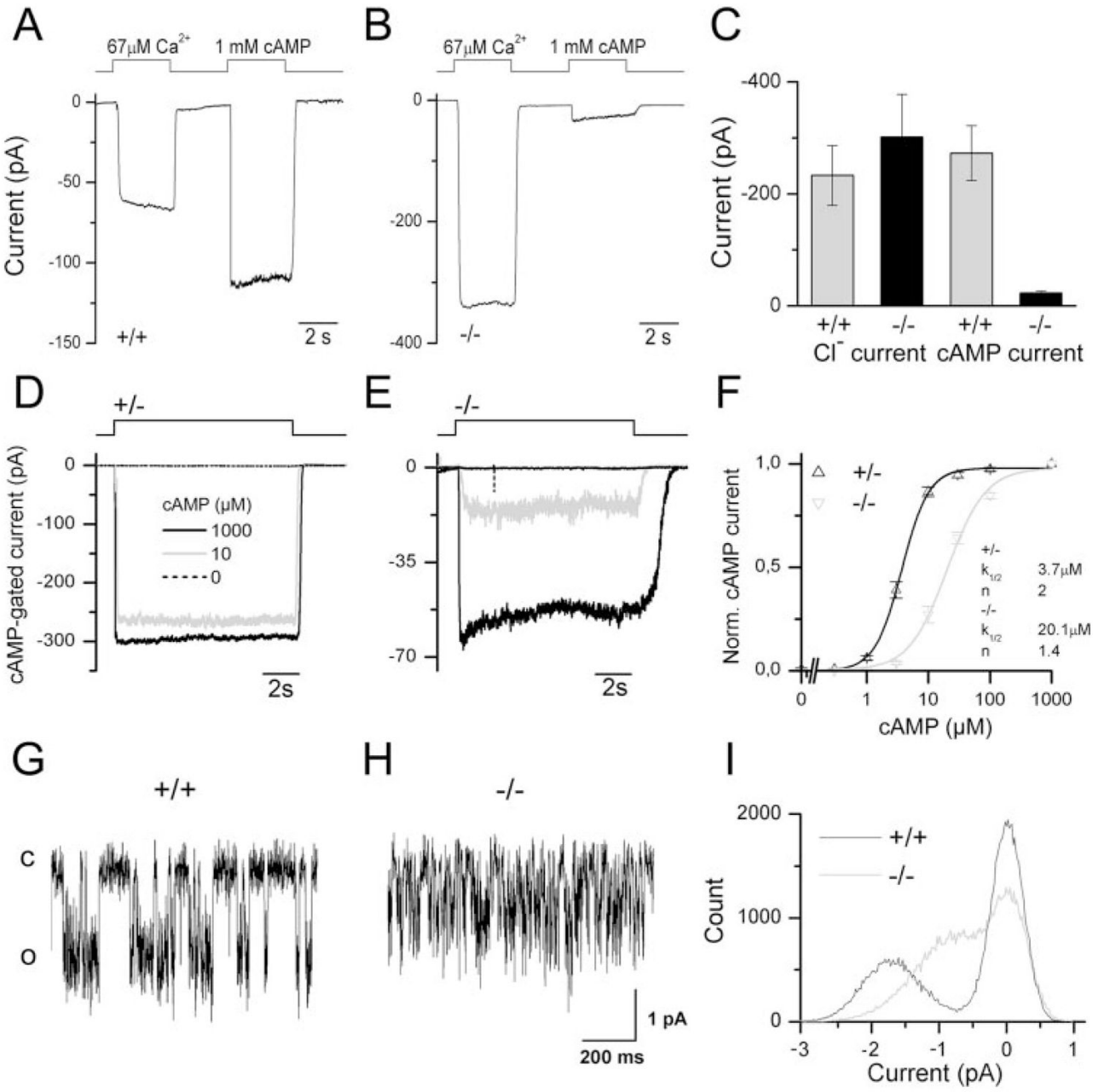

FIGURE 5. The olfactory CNG channel from CNGB1$^{-/-}$ ORNs reveals a reduced peak-current amplitude, a lower cAMP sensitivity, and displays an extremely rapid flicker-gating behavior

Patches excised from dendritic knobs of CNGB1$^{+/+}$ (*A*) and CNGB1$^{-/-}$ (*B*) ORNs were exposed to 67 μ_M Ca^{2+} or 1 m_M cAMP. Because the Cl^- current exhibits "rundown" over time, traces were recorded within 15 s after patch excision. *C*, mean Cl^- and CNG currents in patches from CNGB1$^{+/+}$ and CNGB1$^{-/-}$ mice. Cl^- current: CNGB1$^{+/+}$ 232 ± 53 pA; CNGB1$^{-/-}$, 301 ± 76 pA (n.s.; n = 9). CNG current: CNGB1$^{+/+}$, 273 ± 49 pA; CNGB1b$^{-/-}$, 23 ± 3 pA (p < 0.005; n = 9). *D* and *E*, currents induced by 10 and 1000 μ_M cAMP, respectively, from an excised, inside-out membrane patch from the dendritic knob of a CNGB1$^{+/-}$ (*D*) and a CNGB1$^{-/-}$ (*E*) ORN. *F*, normalized cAMP dose response relationships from CNGB1$^{+/-}$ and CNGB1$^{-/-}$ mice. Currents were determined 10 s after exposure to cAMP. *Solid lines* represent

Hill curves fitted to the data. *G–I*, single channel activity elicited in patches excised from CNGB1$^{+/+}$ (*G*) and CNGB1$^{-/-}$ (*H*) ORNs by applying 3 and 10 μ_M cAMP, respectively. Open (*o*) and closed (*c*) levels are indicated in the figure. *I*, all-point amplitude histogram of 18-s exposures to cAMP of channels from CNGB1$^{+/+}$ (*black trace*) and CNGB1$^{-/-}$ (*gray trace*) ORNs. All experiments were performed in symmetrical NaCl solution at a holding potential of −40 mV (*A–F*) or −60 mV (*G–I*).

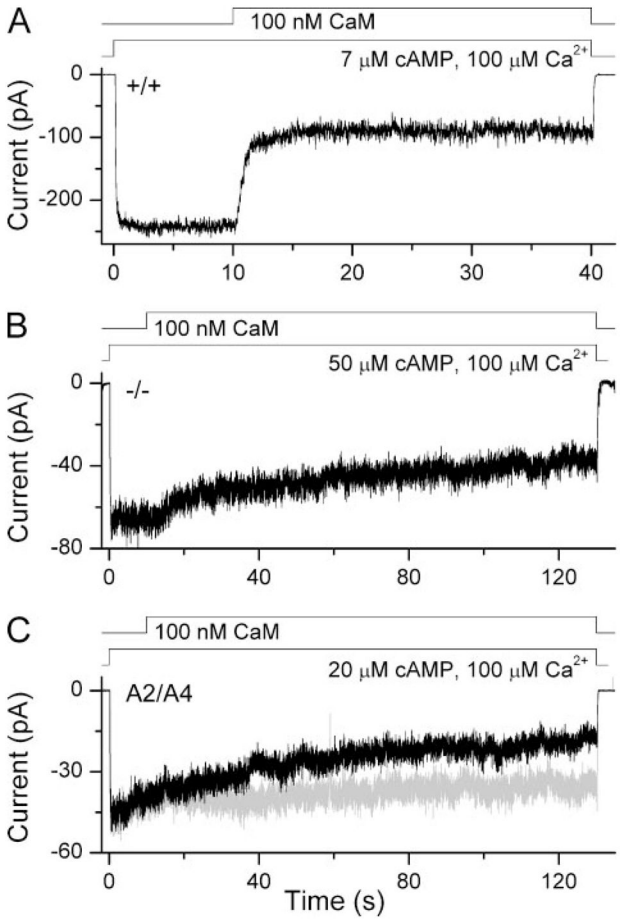

FIGURE 6. Slow inactivation of the CNG channel by Ca^{2+}-CaM in CNGB1$^{-/-}$ ORNs

Patches excised from CNGB1$^{+/+}$ (*A*), CNGB1$^{-/-}$ (*B*) ORNs or HEK293 cells transfected with CNGA2 and CNGA4 (*C*) were exposed to levels of cAMP, chosen to yield an open probability of 0.75 (7, 50, and 20 μ_M cAMP, respectively). Application of Ca^{2+} -CaM quickly reduced the CNG current only in patches from CNGB1$^{+/+}$ ORNs, while channels from CNGB1$^{-/-}$ or heterologously expressed CNGA2/CNGA4 channels showed a similarly slow inactivation. In *C* the *gray trace* represents the current evoked by cAMP in the absence of Ca^{2+} -CaM. All experiments were performed in symmetrical Na-methanesulfonate solution, and the pipette solution contained 1 m_M niflumic acid to suppress the Ca^{2+} -activated Cl^- current.

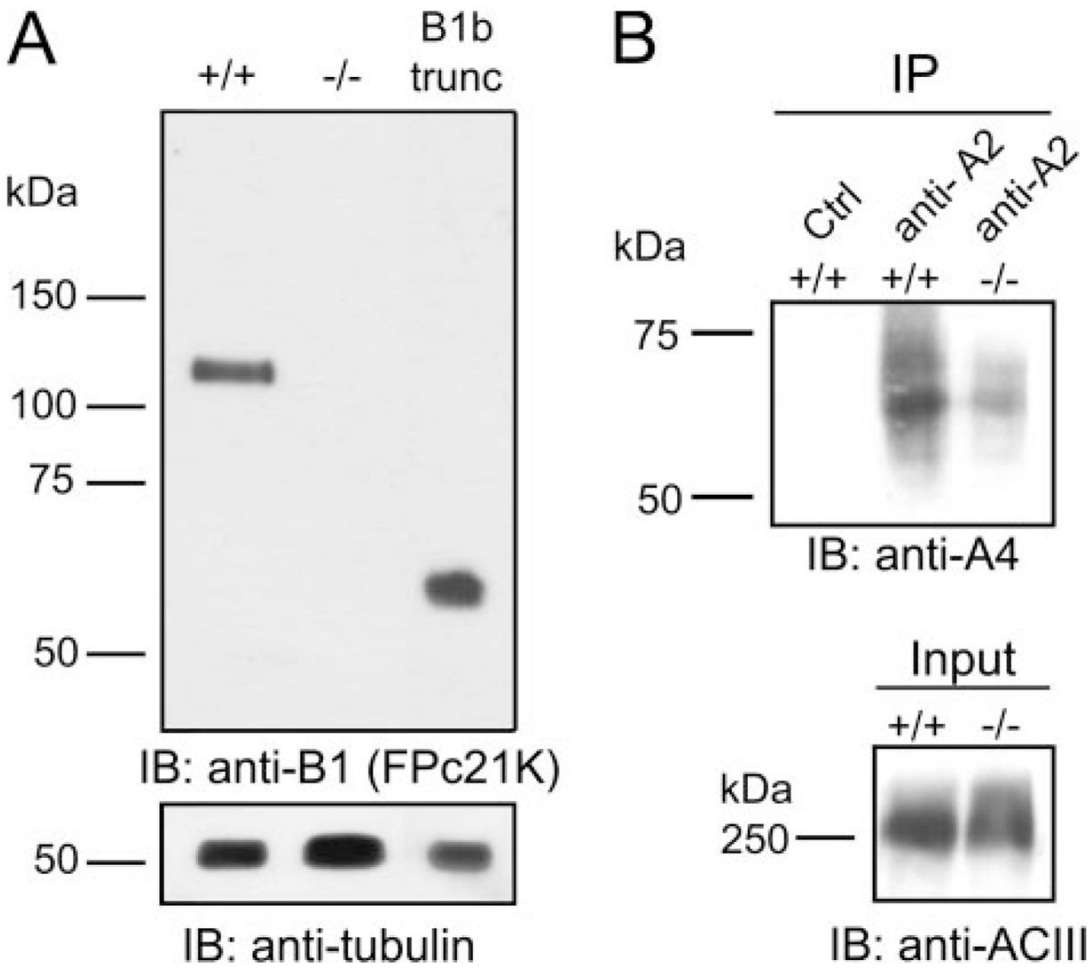

FIGURE 7. Detection of a CNGA2/CNGA4 channel in CNGB1$^{-/-}$ olfactory epithelium

A, top panel: immunoblot of membrane fractions from olfactory tissue of CNGB1$^{+/+}$ or CNGB1$^{-/-}$ mice probed with an antibody directed against the CNGB1b N terminus (FPc21K). Membrane fractions of HEK293 cells expressing a truncated CNGB1b protein (*B1b trunc*) representing the hypothetical gene product encoded by the knock-out-CNGB1 locus are loaded in the *right lane*. *Bottom panel*, same blot probed with anti-tubulin antibody. *B, top panel*, CNGA2 co-immunoprecipitates with CNGA4 in CNGB1$^{+/+}$and CNGB1$^{-/-}$ mice. Equal amounts of membranes from olfactory tissue (210 μg) were precipitated with rabbit anti-CNGA2 (anti-A2) or a control antibody (anti-PAK, Ctrl), respectively, blotted, and probed with guinea pig anti-CNGA4 (anti-A4). *Bottom panel*, loading control representing 15% of the membranes from olfactory tissue used for the co-immunoprecipitation shown in the *top panel* of *B* probed with rabbit anti-adenylyl cyclase III (*ACIII*).

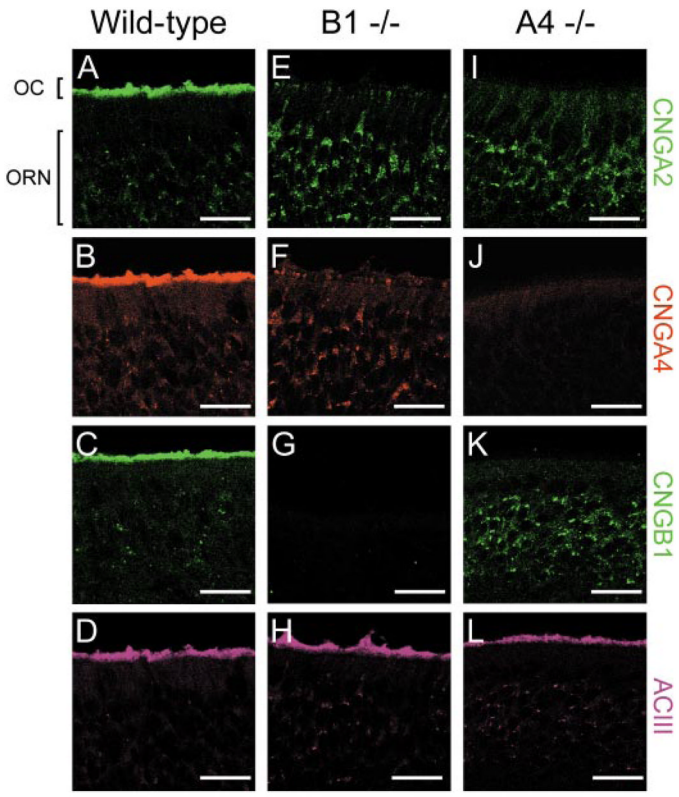

FIGURE 8. Analysis of CNG channel expression in wild-type and mutant olfactory epithelium

Confocal images of sections from 4-week-old wild-type (*WT*) (*A–D*), CNGB1$^{-/-}$ (*E–H*), and CNGA4$^{-/-}$ (*I–L*) mice labeled with antibodies specific for CNGA2, CNGA4, CNGB1, and the adenylyl cyclase (*ACIII*). For detection of CNGB1 an antibody specific for the C terminus was used. Scale bar represents 20 μm. The position of the olfactory cilia (*OC*) and the ORN cell bodies are marked with *brackets* in *A*. Images in panels (*A*, *B*, and *D*), (*E*, *F*, and *H*), and (*J*, *K*, and *L*) were obtained from triple staining using the indicated antibodies.

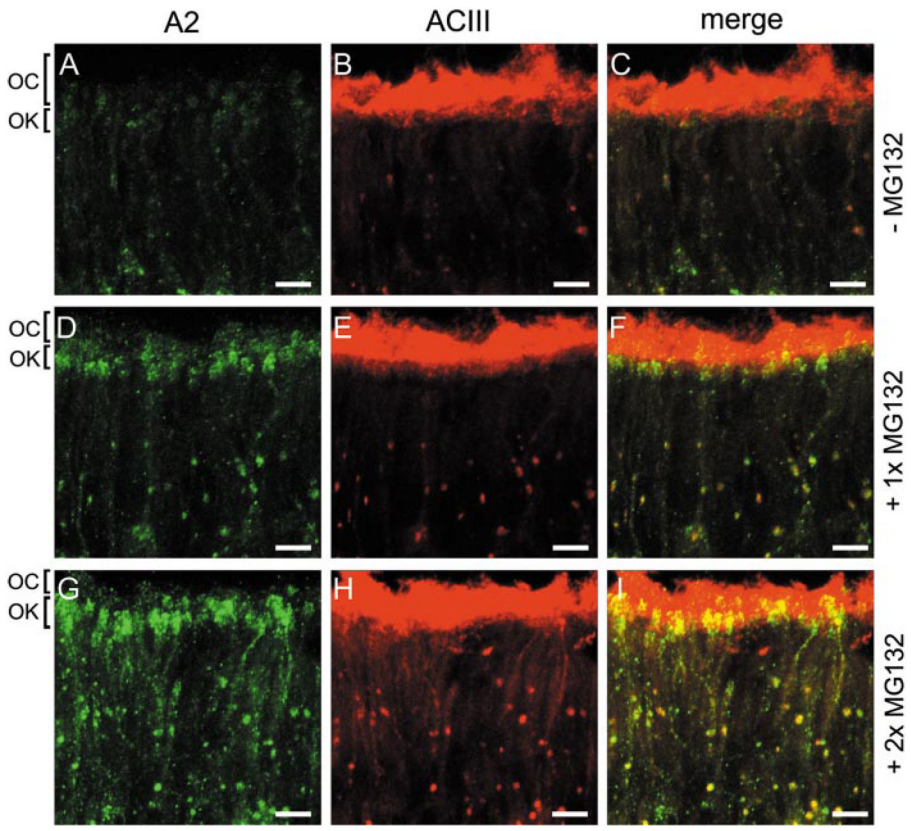

FIGURE 9. Inhibition of the proteasome increases the total CNGA2 protein level in ORNs of CNGB1$^{-/-}$ mice but does not promote targeting of the protein to the cilia

Immunostaining showing the expression of CNGA2 and ACIII in the olfactory epithelium of litter-matched 4-week-old CNGB1$^{-/-}$ mice 20 h after intraperitoneal injection with buffer (*A–C*), with a single dose (10 mg/g) of the proteasome inhibitor MG-132 (*D–F*) or with two doses of MG-132 applied at consecutive days (*G–I*). *Scale bar* is 10 μm. The position of the olfactory cilia (*OC*) and the olfactory knobs (*OK*) are marked with *brackets*. All images are projections of confocal z-stacks.

TABLE 1

Statistical analyses of responses to odorants and forskolin

		Electro-olfactogram		
		CNGB1$^{+/+}$ (n)	**CNGB1$^{-/-}$ (n)**	***t* test**
Onset Recovery	Time to peak (s)	0.66 ± 0.11 (9)[a]	2.82 ± 0.54 (10)	$p < 0.005$
	τ_1[b]	1.16 ± 0.32 (9)	5.72 ± 1.19 (9)	$p < 0.005$
	τ_2	25.10 ± 4.78 (9)	39.59 ± 8.76 (9)	ns[c]
		Forskolin-induced Ca^{2+} signal in ORN knob		
		CNGB1$^{+/+}$ (n)	**CNGB1$^{-/-}$ (n)**	***t* test**
Onset Recovery	Time to peak (s)	8.3 ± 0.5 (29)	13.2 ± 1.3 (34)	$p < 0.005$
	τ	11.7 ± 1.2 (21)	19.7 ± 2.3 (28)	$p < 0.01$

[a] Values are mean ± S.E.

[b] τ, time constant.

[c] ns, not significant.

TABLE 2

Cyclic nucleotide sensitivity of native and heterologously expressed olfactory CNG channels

Values are given as mean ± S.E. Membrane potential was −40 mV for native cells and −60 mV for heterologous expressions.

Type of channel	cAMP			cGMP		
	N[a]	$K_{1/2}$	n[b]	N	$K_{1/2}$	n
		μM			μM	
Native ORNs						
CNGB1$^{+/-}$	6	3.70 ± 0.11	1.99 ± 0.11	5	2.64 ± 0.08	1.88 ± 0.11
CNGB1$^{-/-}$	6	20.15 ± 1.74	1.40 ± 0.14	8	6.90 ± 0.38	1.40 ± 0.09
Expression in HEK293 cells						
CNGA2 + A4 + B1b	7	6.6 ± 0.96	1.55 ± 0.16	10	2.80 ± 0.14	2.40 ± 0.27
CNGA2 + A4	11	17.5 ± 1.22	1.64 ± 0.05	12	3.06 ± 0.16	1.58 ± 0.12

[a] N, number of cells.

[b] n, Hill coefficient.